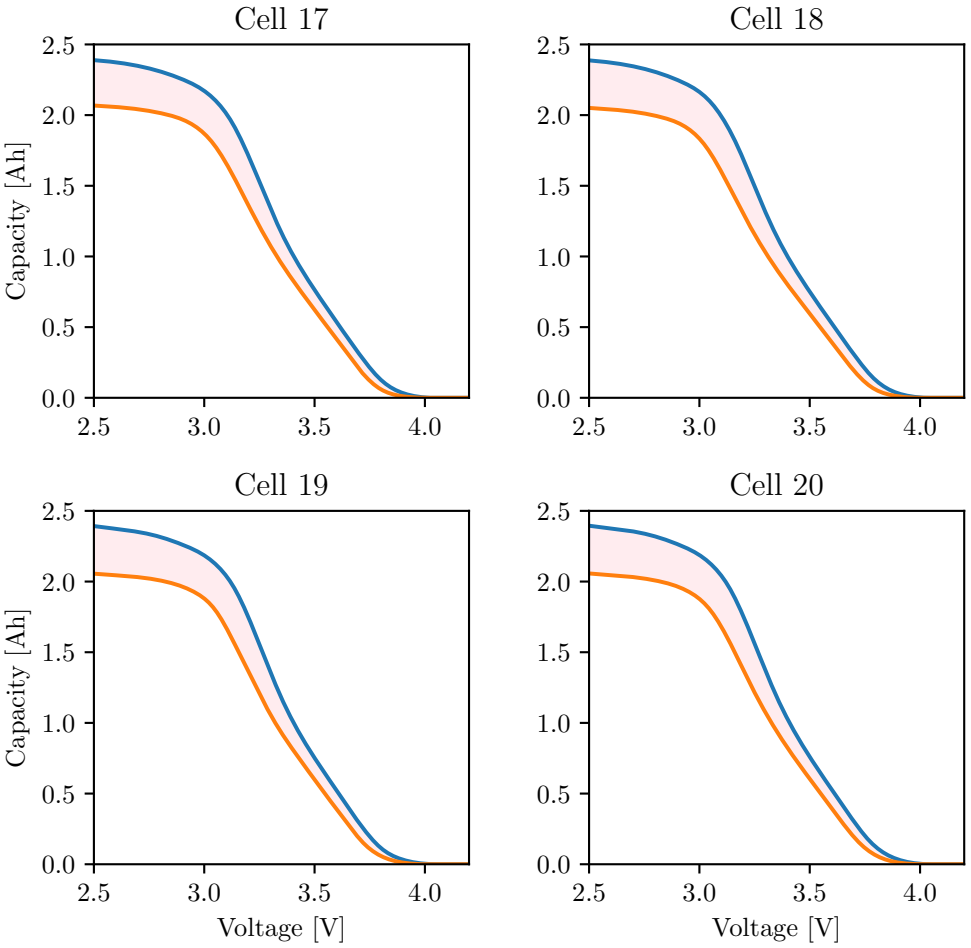

Predicting Cycle Life of NMC Cells by Discharge Capacity Voltage Curves

Master's thesis in Applied Data Science

CHRISTOFFER WIGFORSS

Department of Physics
CHALMERS UNIVERSITY OF TECHNOLOGY
Gothenburg, Sweden 2020

Master's thesis 2020

Predicting Cycle Life of NMC Cells by Discharge Capacity Voltage Curves

CHRISTOFFER WIGFORSS

CHALMERS
UNIVERSITY OF TECHNOLOGY

Department of Physics
Chalmers University of Technology
Gothenburg, Sweden 2020

Predicting Cycle Life of NMC Cells by Discharge Capacity Voltage Curves
CHRISTOFFER WIGFORSS

Supervisor: Kasper Westman, Infotiv AB
Examiner: Patrik Johansson, Department of Physics

Master's Thesis 2020
Department of Physics
Chalmers University of Technology
SE-412 96 Gothenburg
Telephone +46 31-772 10 00

Cover: $Q_{100-10}(V)$ curves

Typeset in LaTeX
Gothenburg, Sweden 2020

Predicting Cycle Life of NMC Cells by Discharge Capacity Voltage Curves
CHRISTOFFER WIGFORSS
Department of Physics
Chalmers University of Technology

Abstract

The biggest issue with rechargeable batteries is arguably their limited lifetime. They suffer from capacity degradation and power fade, and their performance decreases as they age. Estimating the remaining useful life is therefore an important task. However, the complex internal aging mechanisms are difficult to model. Recently, machine learning has become a promising approach for predicting remaining useful life. This thesis evaluates whether a new elastic net machine learning model trained on data from LFP cells can be used to predict cycle life of NMC cells. The model uses capacity and voltage data during discharge phases to derive a feature highly correlated to cycle life. Four commercial NMC cells were cycled in Chalmers Electric Power Battery Lab to collect cycling data. The model was able to make useful cycle life predictions for these cells, which suggests that the approach is applicable to other lithium-ion cells.

Keywords: NMC, cycle life, RUL, prediction, machine learning, elastic net

Acknowledgements

I would like to thank professor Torbjörn Thiringer for letting me use Chalmers Electric Power Battery Lab and helping me with the battery cell testing equipment. I also want to express my gratitude to Research Institutes of Sweden (RISE) for the battery cycling equipment I could borrow.

I would like to thank my examiner professor Patrik Johansson for his advise and for making this thesis possible. I would also like to acknowledge my supervisor Kasper Westman and others at Infotiv, noteworthy Ada Ustundag, even if our beautiful creation was not used in the end and now rests in peace.

Last but not least, I would like to thank my brother Andreas Henriksson for his support with the thesis as well as my wonderful fiancee My Jakobsson, who always has been there for me.

Christoffer Wigforss, Gothenburg, August 2020

Contents

List of Illustrations

Figures

Tables

Acronyms

CC constant current. 5, 6, 13, I
CC-CV constant current-constant voltage. xi, 5, 6, 11, 12, 13, I
CV constant voltage. 5

EoL end of life. 7, 8, 27
EV electrical vehicle. 1

HE4 LG IRC18650-HE4 – The battery cell model used in this experiment. xi, 11, 12, 14, 23, 25, 27, 28

IR internal resistance. 6, 28, I

LFP lithium iron phosphate ($LiFePO_4$). v, 2, 8

M1A A123 APR18650M1A – The battery cell model used in [1]. xi, 8, 9, 12, 14, 15, 23, 25, 27, 28
MPE mean percentage error. xi, 8, 24, 25, 27

NMC lithium nickel manganese cobalt oxide ($LiNiMnCoO_2$). v, 1, 2, 11, 29

RMSE root mean squared error. 24
RPT reference performance test. 7, 13, 19, 28, I, III
RSS residual sum of squares. 10
RUL remaining useful life. v, 2, 3, 7, 8, 25, 27, 29

SoC state of charge. 4, 5, 6, 7, 8, 12, 13, 27, I
SoH state of health. 6, 7, 8, 13, 17, 27

1

Introduction

Batteries are used everywhere today – in mobile phones, laptops, cars, etc. More and more portable devices are produced with a need for power supply without the restriction of having to be connected to an electrical outlet, and adding batteries to such devices is a natural choice.

In the last two decades, there has been a rapid development and increase of electrical vehicles (EVs), e.g. cars, buses and trucks, and recently also battery powered airplanes [2] with no gas emissions compared to vehicles with combustion engines. Batteries are suitable for these applications to transition from fossil fuels to more sustainable alternatives for transporting people and goods.

Even if batteries were invented already around year 1800 [3] and much research has been done since then, there still are a number of issues to solve. The biggest one is arguably the limited lifetime of rechargeable batteries, which age and degrade over time. Their capacity decreases and the performance gets unreliable as they get older.

This is for example a major issue for EVs, where the battery is an essential part of the vehicle since the capacity of the battery is directly correlated to the driving range. A lower maximum capacity implies shorter distance on a full charge, and a degradation of the capacity would be the same as a gas tank shrinking by time as the vehicle gets older. To counteract this, some car manufacturers oversize the battery to make the maximum driving distance seem constant to the customer during the car's service life, hiding and delaying the effects of degradation [4]. The result of this is a larger battery at a even higher price and more mass to transport which is not even fully utilized until much later.

One of the most common battery chemistries in EVs is lithium nickel manganese cobalt oxide ($LiNiMnCoO_2$) (NMC) [5, 6] since it has high capacity and lower production cost compared to other alternatives. However, in addition to suffering from capacity degradation and power fade, NMC cells are not so stable [7]. Numerous battery fire and thermal runaway incidents in EVs have been reported [8]. Some incidents are caused by crashes, in which the fragile battery gets damaged, but most of the failures are due to misuse. This includes high charge and discharge speeds, usage in high temperatures and overcharging. All of them increase the risk of over-

heating and short circuiting, which may cause batteries to catch fire or even explode [9, 10].

The probabilities for such events also increase as a battery ages. Therefore, it is important to estimate the remaining useful life (RUL) to know when to replace batteries.

Unfortunately, degradation in lithium-ion batteries is a complex, nonlinear process. Modeling it requires knowledge about properties of the internal materials, the chemical reactions as well as different aging phenomena, involving many parameters and heavy computations. Another approach is the data-driven approach, where historical data is the source of knowledge. Much research on making RUL predictions using machine learning models trained on such data has been done recently [11], and this thesis explores that research area further.

1.1 Aim

The goal of this project is to predict the cycle life of NMC battery cells using the variance model developed for lithium iron phosphate ($LiFePO_4$) (LFP) cells by Severson et al. [1] and evaluate whether that model can be used for commercial NMC cells.

1.2 Limitations

Limited time and limited resources limits the number of battery cells cycled and included in the analysis. The focus will also be only one of the many variants of NMC cells, namely $Ni_{1/3}Mn_{1/3}Co_{1/3}$.

2

Theory and Model

This chapter will introduce batteries and related fundamental theory. RUL of batteries will be discussed, and methods for predicting RUL will be explained.

2.1 Batteries

A battery is a device that stores chemical energy which can be transformed into electrical energy [12]. This section will introduce batteries and their internal parts, common concepts and aging of batteries.

2.1.1 Components and Chemistry

Even though a battery is most commonly referred to as one single unit, it generally consists of several cells connected in series and/or in parallel depending on the application [12].

Figure 2.1 illustrates the components of a cell. Each cell has a positive and a negative electrode, called cathode and anode. This is where the lithium ions are stored. The electrodes are connected by an electrolyte, which allows ions to move between them. If the two electrodes were to be in direct contact with each other, the cell would be short-circuited. To prevent that from happening, a separator in the electrolyte prevents contact between the two poles.

Ions at the anode want to move to the cathode based on the size of the free energy difference between the electrodes, which creates a potential over the cell. The potential corresponds to the voltage, measured in volts (V) and denoted by the mathematical variable V.

The voltage is determined by the composition and structure of materials of the electrodes – the "active" materials. This, together with the "inactive" materials (electrolyte, separator and current collectors) and how cells are organized, also defines a battery's other characteristics, such as energy density (weight and volume) and power throughput.

In lithium-ion batteries, the positive electrode is a metal-oxide while the negative electrode is made of carbon, e.g. graphite. The electrolyte is an organic liquid in

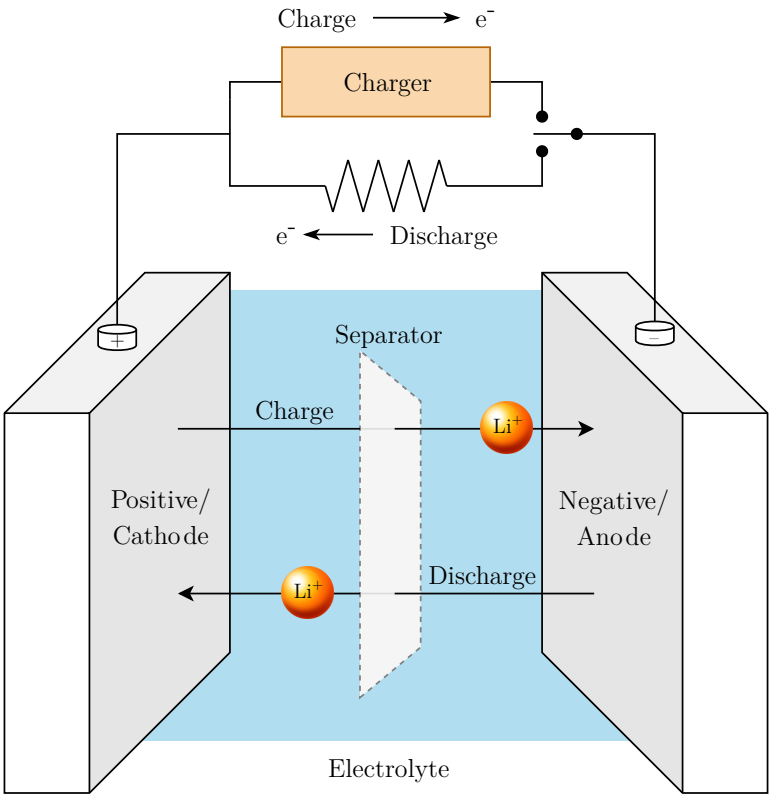

Figure 2.1: Components inside a battery cell and the flow of Li-ions and electrons during charge and discharge

which lithium salts have been dissolved. [13]

2.1.2 Charging and Discharging

The transformation from chemical energy to electrical energy is driven by oxidation-reduction (redox) reactions between the materials inside the battery while electrons can flow through a circuit connected to the battery [12]. When a battery is used to power something, lithium ions stored at the negative electrode simultaneously move to the positive electrode.

In rechargeable batteries, these redox reactions can be reversed by connecting a power supply [12]. The lithium ions then move in the opposite direction, restoring the battery's condition to a charged state and making it possible for the redox reactions to occur again.

The capacity of a battery is measured in ampere hours (Ah), denoted by Q. The fraction between the current and maximum capacity is defined as state of charge (SoC). To an end user, this is equivalent to the percentage remaining in for instance their mobile phone's or laptop's battery. The definition is given in Equation 2.1.

$$\text{SoC} = \frac{Q_{\text{current}}}{Q_{\text{max}}} \tag{2.1}$$

How fast a cell is charged or discharged is determined by the current, the flow of electrons, between the electrodes of the cell. Different cells can handle currents of different magnitudes. To be able to compare charge and discharge speeds regardless of battery capacity, one can use the notation of C-rates, denoting the amount of current relative to the design capacity of a specific cell. C-rates are inversely proportional to the time it takes to completely charge a cell, and a higher rate means higher current and, hence, shorter charging time (Figure 2.2). A C-rate of 1 implies a full charge from 0 % to 100 % in one hour, 2C charges the cell in 30 minutes while it takes 120 minutes to charge with a C-rate of 0.5C. C-rates are used in the same manner for discharge speeds.

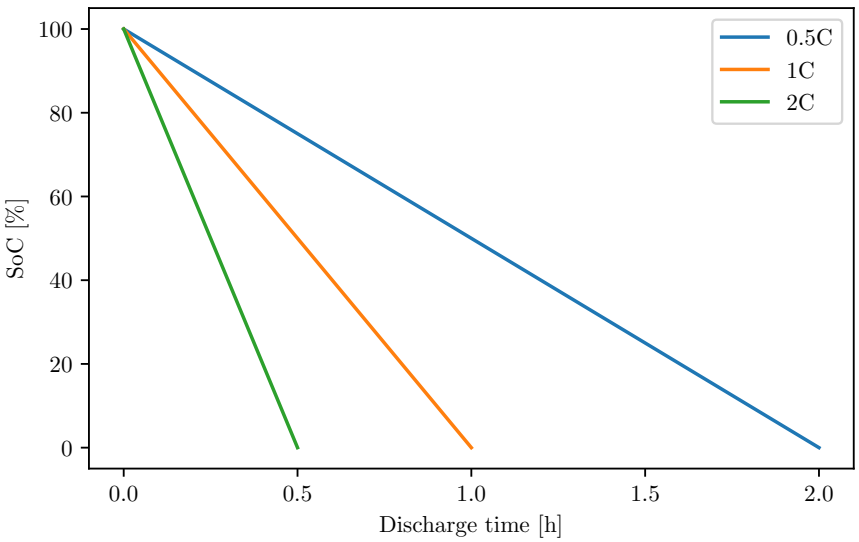

Figure 2.2: Discharge time for different C-rates

A common approach to charge Li-ion cells is a constant current-constant voltage (CC-CV) procedure. It has two phases, where the charger in the first phase applies constant current (CC) until the cell hits its upper voltage limit. This phase corresponds to the three CC regions (red, orange and yellow) in Figure 2.3 where the current is constant and the voltage is below 4.2 V. To prevent overcharging, the voltage is kept constant in the constant voltage (CV) phase, and the current decreases gradually. When the cell accepts a pre-defined cut-off current, the charging is stopped.

Discharging can be executed in a similar procedure. A constant current can be withdrawn from the cell until the voltage reaches the lower limit. After that, the voltage can be kept constant while the current decreases.

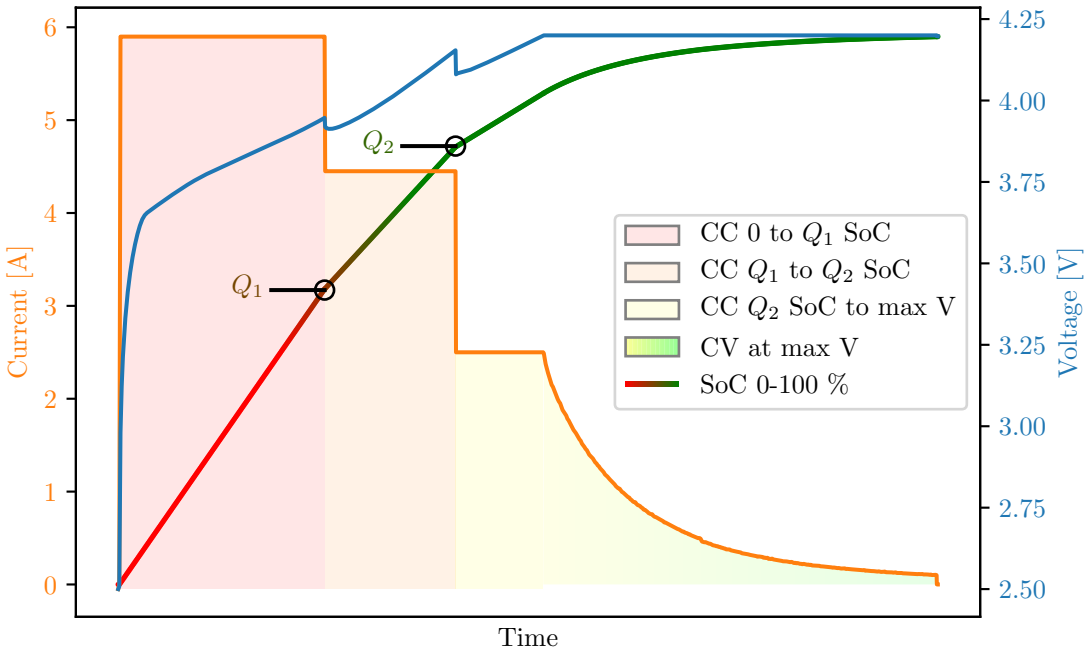

Figure 2.3: A multistage CC-CV charging example with three CC stages. The current is changed at two SoC levels, Q_1 and Q_2.

2.1.3 Aging

Even though the redox reactions in rechargeable batteries are reversible, they are not completely so. Changes to the internal materials will decrease the cells' performance in terms of how much energy they can store and deliver. These changes are more likely to happen when a cell is exposed to low or high temperatures or low or high SoC levels [13, 14].

As a cell ages, different degradation mechanisms make it harder for the cell to operate efficiently. The main consequences of degradation are capacity fade and power fade [14], meaning shorter use time and instability issues. This is caused by, inter alia, increase of the internal resistance (IR) in the cell due to weaker contact between the internal components [14], which generates a lot of heat during use. High temperatures, in turn, causes more damage to the cell, hasting the aging process additionally.

State of health (SoH) is a measure of how much a battery cell has degraded. One of the most common definitions is a ratio between the current maximum capacity and the rated, initial capacity [15], as in Equation 2.2.

$$\text{SoH} = \frac{Q_{\text{max}}}{Q_{\text{rated}}} \tag{2.2}$$

When a cell's SoH has reached a certain level, the cell is considered to have reached

its end of life (EoL). This level may be different from application to application, since applications have different requirements on the power supply, but a SoH of 80 % is most often used as the condition in the context of capacity as above [16].

2.2 Remaining Useful Life Prediction

In the context of battery aging, the number of cycles a battery has made is often discussed. A full cycle is completed when a battery has discharged from 100 % to 0 % SoC and recharged back to 100 % again. This is most often not the case in real life though. Instead, equivalent full cycles (EFCs) are used to count accumulated energy during charging and discharging that is equivalent to the energy of a full cycle [17], as in Figure 2.4.

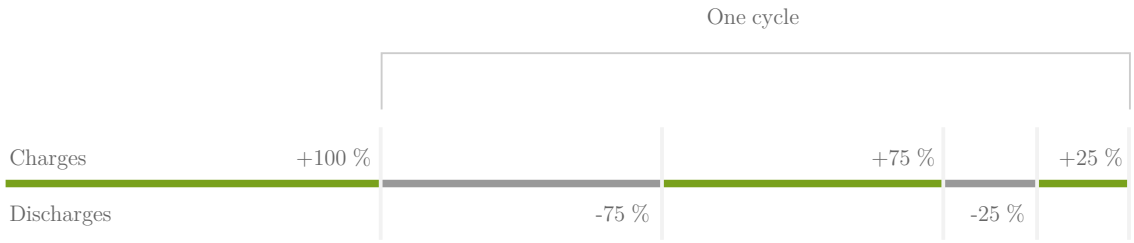

Figure 2.4: Example of an equivalent full cycle

The number of cycles a battery has completed does not alone say how healthy it is. An analogy for humans would be the saying "the age of a person is just a number". How the battery has been treated and what it has been exposed to is more important. However, since the usage of a battery affects the cycle life, the number of cycles a battery has performed is a good indicator of its age and health.

Knowing when a battery cannot meet its performance requirements anymore could be crucial for some applications [18]. This is why remaining useful life (RUL) prediction for batteries is important and has gained more and more focus recently [19–21]. However, modeling and predicting the complex degradation mechanisms inside lithium-ion batteries is complicated since they are not visible from the outside and difficult to measure.

2.2.1 Incremental Capacity Analysis and Differential Voltage Analysis

To see changes in a cell's internal materials, one can perform reference performance tests (RPTs). Such tests reveal reactions in the cell at different stages during a slow charge or discharge, and how these reactions evolve over time gives an indication of how the materials have been affected and different aging phenomena.

Voltage and capacity data from this type of (dis)charges are used to perform incremental capacity analysis (ICA) and differential voltage analysis (DVA). This is

done by visually inspecting derivatives of $Q(V)$ and $V(Q)$ curves, i.e. $\mathrm{d}V/\mathrm{d}Q$ and $\mathrm{d}Q/\mathrm{d}V$ – a technique to identify aging mechanisms in Li-ion cells [22–24].

ICA and DVA have also proven to be powerful for estimating SoH [25–28]. This is interesting since voltage and capacity measurements are relatively easy to obtain.

2.3 The Variance Model

$Q(V)$ curves and features derived from them have also been used for predicting RUL. One feature in particular has shown to have a strong correlation to the cycle life.

In a study [1] by Severson et al., who cycled and collected data from 124 lithium iron phosphate ($LiFePO_4$) (LFP) cells, three models were developed and trained to predict cycle life. The models are elastic nets, a type of machine learning model explained in subsection 2.3.1, with no prior knowledge of degradation mechanisms and rely entirely on the underlying data.

The data was collected by cycling the 124 cells (A123 APR18650M1A, hereafter referred to as M1A) from 0 % to 100 % SoC using 72 different fast charging policies and then equally discharged back to 0 % at 4C. This was performed in a temperature chamber at 30 °C. The cycle life of the cells ranged from 150 to 2,300 with an average of 806 cycles before their SoH reached 80 %, which was set as the end of life (EoL) criterion.

One of the proposed features, selected in all three models, uses voltage and capacity measurements from the collected data. The discharge capacity during the discharge phase of cycle 10 and 100 is fitted as a function of the voltage for the capacity values, $Q(V)$. This results in two curves for the two cycles, $Q_{10}(V)$ and $Q_{100}(V)$. An example is shown in Figure 2.5. Severson et al. found that the difference of these discharge curves, $\Delta Q_{100-10}(V)$, which yields a function as well, contains useful information that has a strong relation to the number of cycles for a battery cell. The logarithm of the variance of that resulting function, $\log_{10}(\mathrm{Var}(\Delta Q_{100-10}(V)))$, was linearly correlated to the logarithm of the number of cycles with a correlation coefficient $\rho = -0.92$.

For one of the models, the “variance” model, that feature was the only feature. Even though the model is so simple, it still achieves a mean percentage error (MPE) of 11.4 % when predicting cycle life of the 40 cells part of the test dataset. This makes the model of special interest since it is both noncomplex and very efficient. Therefore, the variance model will be the focus of this thesis.

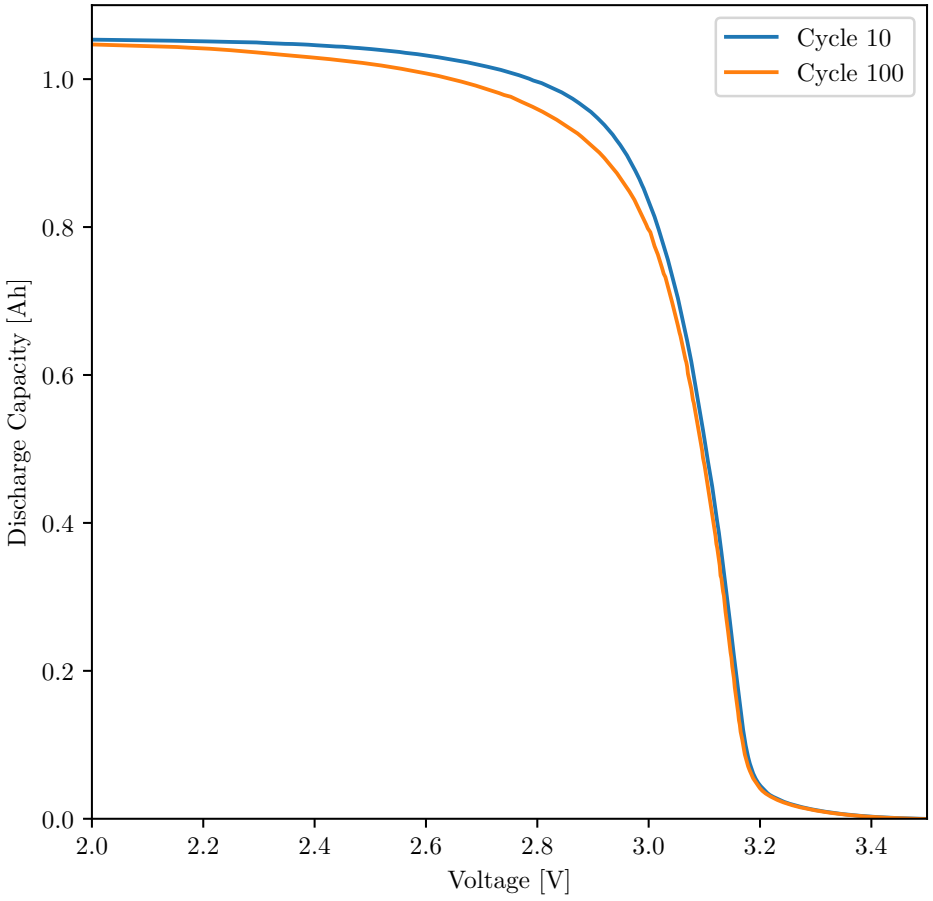

Figure 2.5: $Q(V)$ curves for a M1A cell

2.3.1 Elastic Nets

The variance model introduced in section 2.3 is an elastic net, a type of linear regression model proposed by Zou and Hastie in 2005 [29], where the goal is to find and fit an optimal line between a set of data points. The model can then be used to estimate numerical values for new, unseen data.

The representation of an elastic net can be seen in Equation 2.3, where all k features $x_1, x_2, ..., x_k$ have their own weight $w_1, w_2, ..., w_k$.

$$y = w_0 + w_1x_1 + w_2x_2 + ... + w_kx_k \tag{2.3}$$

Training an elastic net means finding optimal values for the weights which will minimize the value of a cost function. In the context of linear regression, the cost

function is the residual sum of squares (RSS), i.e. the sum of squared errors between the model's estimated values and the true values. The formula for RSS is given in Equation 2.4, where $\hat{y}_i$ and y_i are the predicted and the true value respectively for data point i in a set of n data points.

$$\text{RSS} = \sum_{i=1}^{n} (\hat{y}_i - y_i)^2 \tag{2.4}$$

Minimizing the cost function is done by running the gradient descent optimization algorithm, which iteratively finds local minimum optima for the function and thus also optimal combinations of weights. However, in elastic nets, the RSS is not the only thing that is minimized. Elastic nets also utilizes a mix of two regularization methods, lasso and ridge, which serve to reduce the error and the complexity of the model. Lasso, or L_1 regularization, adds a penalty of the absolute sum of the weights to the cost function while ridge, or L_2 regularization, adds the sum of squared weights. Their definitions are given in Equation 2.5 and Equation 2.6.

$$L_1 = \sum_{j=1}^{k} |w_j| \tag{2.5}$$

$$L_2 = \sum_{j=1}^{k} {w_j}^2 \tag{2.6}$$

The resulting cost function thus becomes

$$\sum_{i=1}^{n} (\hat{y}_i - y_i)^2 + \lambda \sum_{j=1}^{k} |w_j| + (1 - \lambda) \sum_{j=1}^{k} {w_j}^2$$

where λ is a parameter between 0 and 1 that controls the ratio between the lasso and ridge penalties. An additional parameter α can be added to the L_1 and L_2 terms to control the overall importance of them.

The two regularization methods have different advantages and disadvantages. Lasso does feature selection and helps producing sparse models by eliminating less important variables. This may often be desirable, but can remove useful information such as multicollinearity. Ridge, on the other hand, may mark features as less important but keeps them and makes models dense and hard to interpret.

By using a combination of both methods, elastic nets overcome the limitations of each one of them. This also leads to the additional advantage that elastic nets are powerful when the number of features is much larger than the number of data points in the dataset. For this reason, elastic nets are suitable when modeling complex systems such as aging of lithium-ion batteries, where numerous factors and processes affect the aging process.

3

Method

Four lithium nickel manganese cobalt oxide ($LiNiMnCoO_2$) (NMC) battery cells were cycled in Chalmers Electric Power Battery Lab to collect cycling data. Data from the 100 first cycles was used to predict the remaining number of cycles for each cell using the variance model described in section 2.3. The data collection method and how the data was processed are described in the sections below.

3.1 Battery Cycling

Specifications of the cell model and the equipment used for cycling is detailed in this section. How the cells were cycled is also specified.

3.1.1 Cell Type

The cells used in this experiment were LG ICR18650-HE4 (hereafter referred to as HE4), which is a power optimized NMC ($Ni_{1/3}Mn_{1/3}Co_{1/3}$) cell of size 18650 with a nominal capacity of 2,500 mAh and a manufacturer defined voltage range from 2.5 to 4.2 V. The recommended fast charging method of these cells is a CC-CV of 4 A (1.6C) with a 100 mA end-current cut-off.

3.1.2 Hardware

The cells were mounted in holders (Figure 3.1a) connected to a PEC ACT0550 cell tester in four different channels: 17, 18, 19 and 20. For simplicity, the cells in this experiment are referenced by their channel number.

In contrast to the experiment [1] by Severson et al., no temperature chamber was used. Instead, axial fans (Figure 3.1b) were placed above each holder to air-cool the cells in a room with an ambient temperature of ca 24 °C. The temperature was then monitored with a temperature sensor attached to the side of each cell.

3.1.3 Cycling Protocols

The cells were cycled according to two cycling protocols, A and B, based on two of the fast charging protocols used in the reference study [1]. The chosen original

a. b.

Figure 3.1: Photos of a HE4 cell inside a holder adjusted for cells of size 18650. One of the axial fans is marked in the second photo.

protocols were two of the protocols for M1A cells with the highest cycle life prediction accuracy. Two were chosen since it would give a small variety while still having redundancy for errors.

The protocols consisted of full cycles from 0 % to 100 % SoC in two or three stages with different C-rates followed by a complete CC-CV discharge back to 0 % SoC (Figure 3.2). In protocol A, the current was changed during charging at two different SoC levels, Q_1 and Q_2. For protocol B, the current was changed only once, at Q_2. The values for Q_1 and Q_2 are listed in Table 3.1. From Q_2 to 100 % SoC, the cells were charged with CC-CV at 1C with a cut-off of 100 mA.

Protocol	Q_1	Q_2
A	54 %	80 %
B	-	80 %

Table 3.1: Q values for protocol A and B

The goal was to mimic the method of the experiment [1] and to reduce the number of differences in order to achieve comparable results. However, since the type of battery cells in this experiment differs from [1], the C-rates were scaled to match the HE4 cells. The C-rate during discharge for the M1A cells (4C) was below the maximum recommended discharge speed for the HE4 cells and could therefore safely be used in this experiment as well. On the other hand, the C-rates during charge were much higher than the maximum recommended charge speed and would pose a danger if they were to be applied to the HE4 cells. A ratio between the recommended maximum fast charging current for the M1A cells and the C-rates in the protocols was used to compute the C-rates during charging for the HE4 cells. The scaling is shown in Table 3.2.

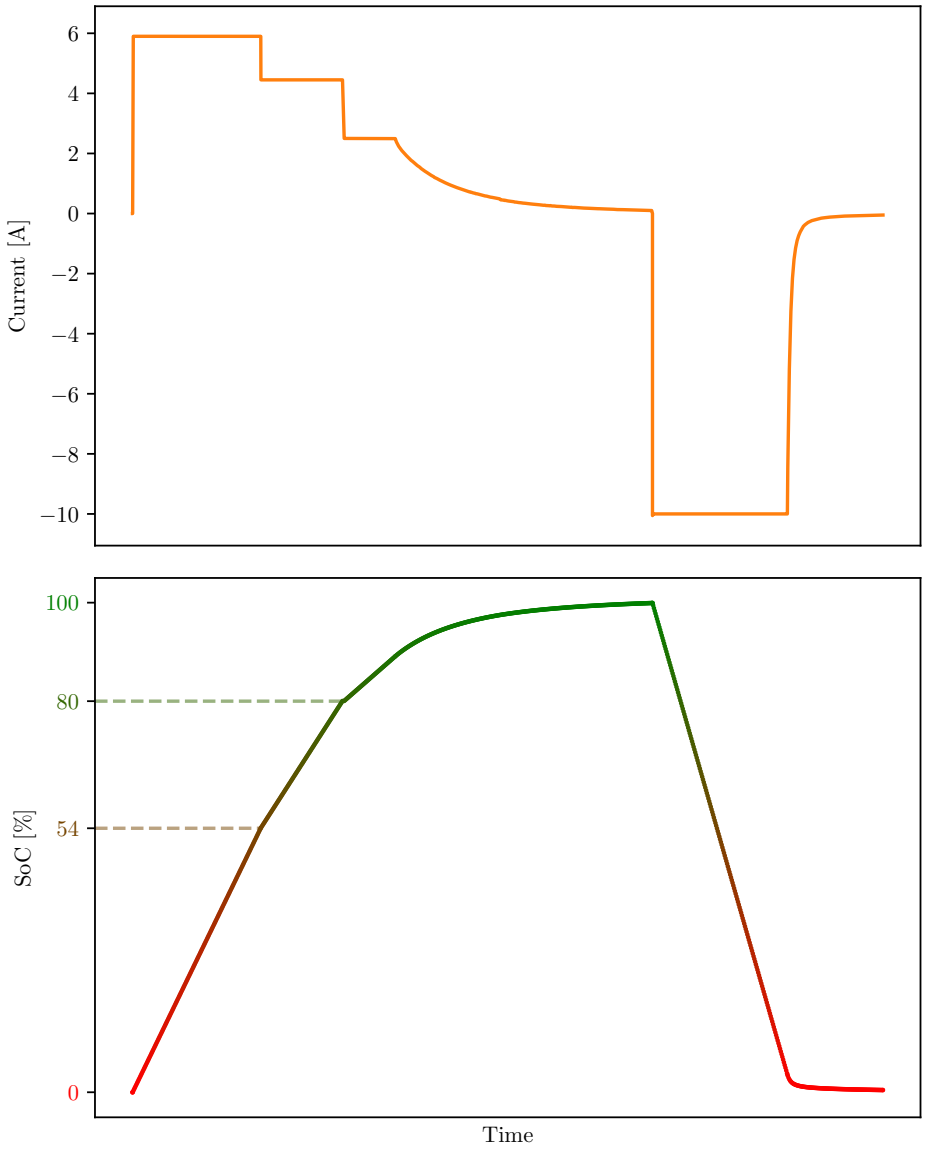

Figure 3.2: Current and SoC as functions of time during a cycle in protocol A

Voltage, current and temperature measurements were recorded every fifth second. Moreover, the internal aging process was also monitored by performing RPTs after cycle 10 and cycle 100. In the RPT, the cells first rested for 2 hours. The cells were then charged with CC-CV at 0.5C with a cut-off of 50 mA. Lastly, the cells were discharged with CC at 0.1C until the voltage hit 2.5 V.

When a cell reached 80 % SoH, the cycling was stopped. This was defined as when the cell could not deliver 80 % of the initial capacity, i.e. $0.8 \cdot 2{,}500$ mAh $= 2{,}000$ mAh, when fully discharged from 100 % SoC.

A flowchart of a test regime is available in Appendix B.

Protocol	APR18650M1A (max 3.6C)		C-rate Ratio		ICR18650-HE4 (max 1.6C)		
	Stage 1	Stage 2	Stage 1	Stage 2	Stage 1	Stage 2	Cells
A	5.3C	4C	1.47	1.11	2.36C	1.78C	17, 18
B	4.8C	4.8C	1.33	1.33	2.13C	2.13C	19, 20

Table 3.2: Specification and conversion of C-rates for M1A and HE4 cells. The C-rates in the parentheses are the recommended maximum fast charging rates specified by the manufacturer.

3.2 Software

The machine learning model was implemented in Python using `ElasticNetCV` from the scikit-learn[1] package. The SciPy library[2] provided functions for interpolating the $Q(V)$ curves.

The dataset published by Severson et al. from their experiment [1] could surprisingly enough not be used to reproduce the results presented in the paper. The discharge capacity voltage curves from cycle 10 and 100 provided in the data do not yield the stated $\Delta Q_{100-10}(V)$ curves, and thus also incorrect values of the feature $\mathrm{Var}(\Delta Q_{100-10}(V))$ as well as bad prediction accuracy. The differences can be seen by comparing Figure 3.3 with the paper's Figure 2b.

Instead, the elastic net was trained on the pre-computed data points extracted from the paper's PDF file when converted to SVG data. This gave the same accuracy metrics when the reconstructed model was evaluated on the test data.

The cycling protocols were implemented in MWare[3] to program to the PEC machine. The C-rates derived from Table 3.2 were converted to currents based on the rated capacity by the cell manufacturer. The test regimes are available in Appendix A.

[1] `https://scikit-learn.org/`
[2] `https://scipy.org/scipylib/`
[3] `http://www.mware-mes.com/`

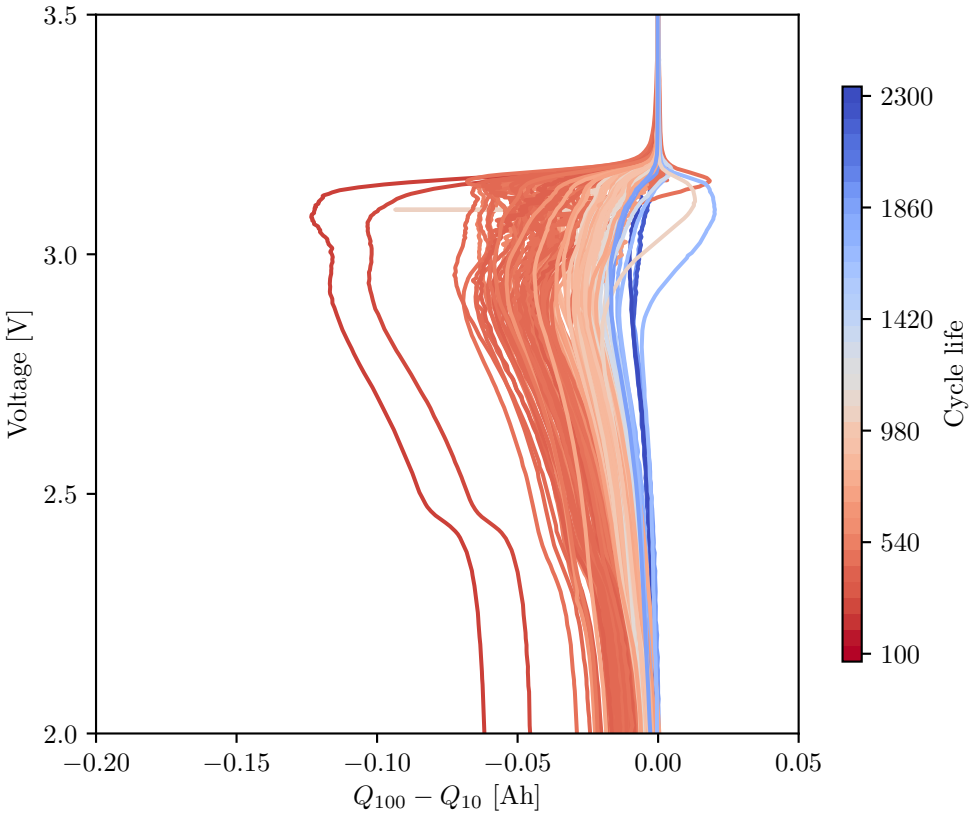

Figure 3.3: $\Delta Q_{100-10}(V)$ curves for the M1A cells

4

Results

4.1 Cycling Data

The cells performed 153, 137, 138 and 140 cycles respectively before their SoH reached 80 % (Figure 4.1). This gives an average of 142 cycles.

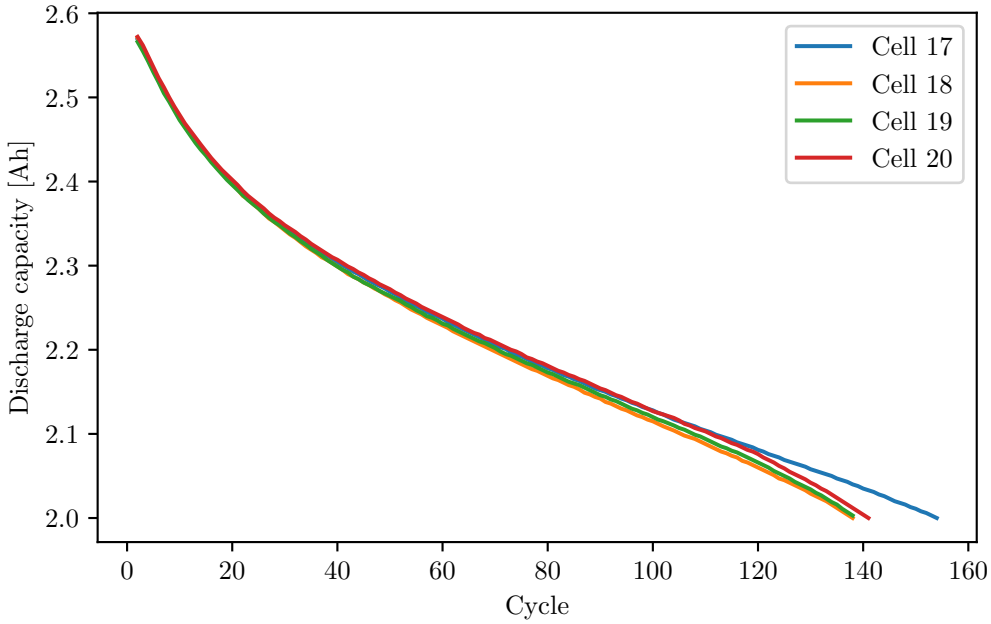

Figure 4.1: Discharge capacity degradation

The temperature increase at the side of the cells during charging was 3-4 °C above ambient temperature in the beginning of the cells' cycle life. Towards the end, this increase rose by 1-2 °C. Much more heat was generated during the discharge phases. The peaks were 10-12 °C above ambient temperature at start and ranged from 12 to 15 °C in the end, i.e. 36-39 °C. The peak temperatures during charge and discharge is shown in Figure 4.2 and Figure 4.3.

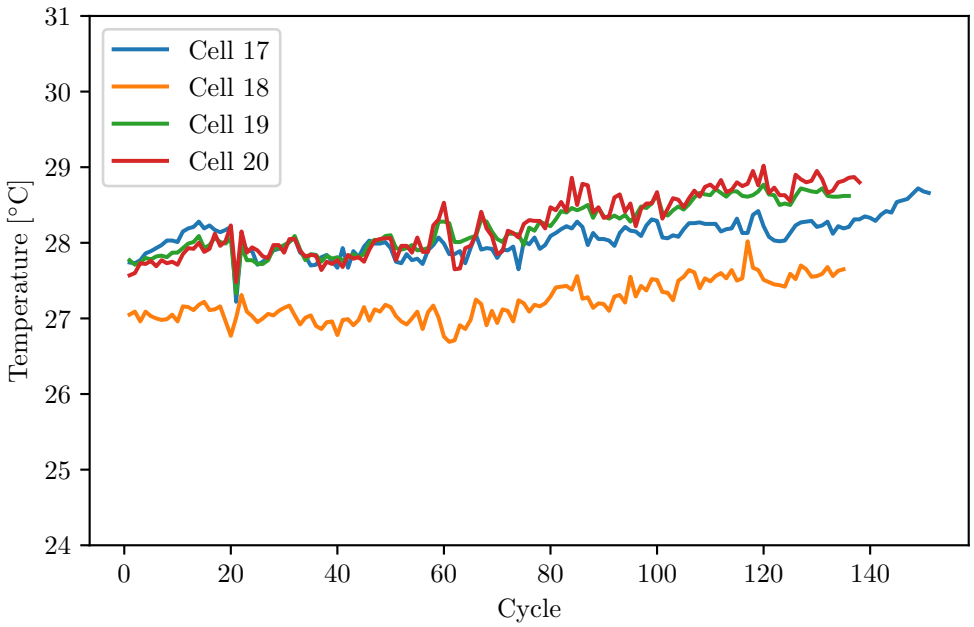

Figure 4.2: Charge temperature peaks during each cycle

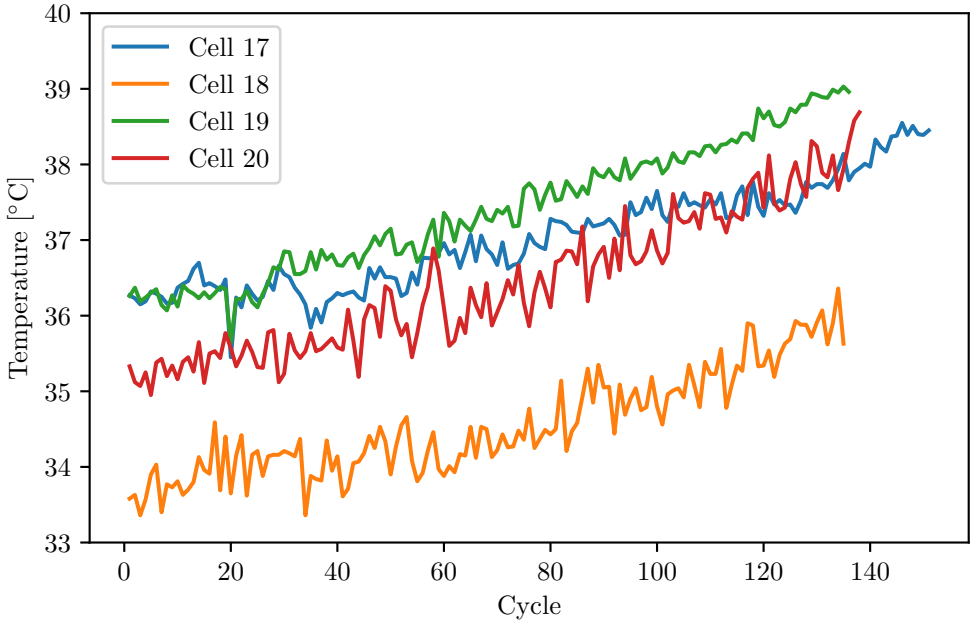

Figure 4.3: Discharge temperature peaks during each cycle

The cells' initial capacities, retrieved from the charge and discharge capacities of the first cycle, are listed in Table 4.1. On average, this is 115 mAh (4.6 %) and 70 mAh (2.78 %) above the nominal capacity of the cells. The nominal capacity of 2.5 Ah was not reached until after 8-9 cycles.

Cell	17	18	19	20	Average
Charge capacity [Ah]	2.650	2.604	2.599	2.607	2.615
Discharge capacity [Ah]	2.569	2.571	2.566	2.572	2.570

Table 4.1: Initial capacities

The first RPTs after cycle 10 took almost 14 hours. The second ones lasted for nearly 12.5 hours.

4.2 Model Predictions

Discharge capacity voltage curves for five cycles are plotted in Figure 4.4 for cell 17. The discharge capacity decreases as the cell ages, but the shape of the curve remains the same. The results for the other cells are very similar.

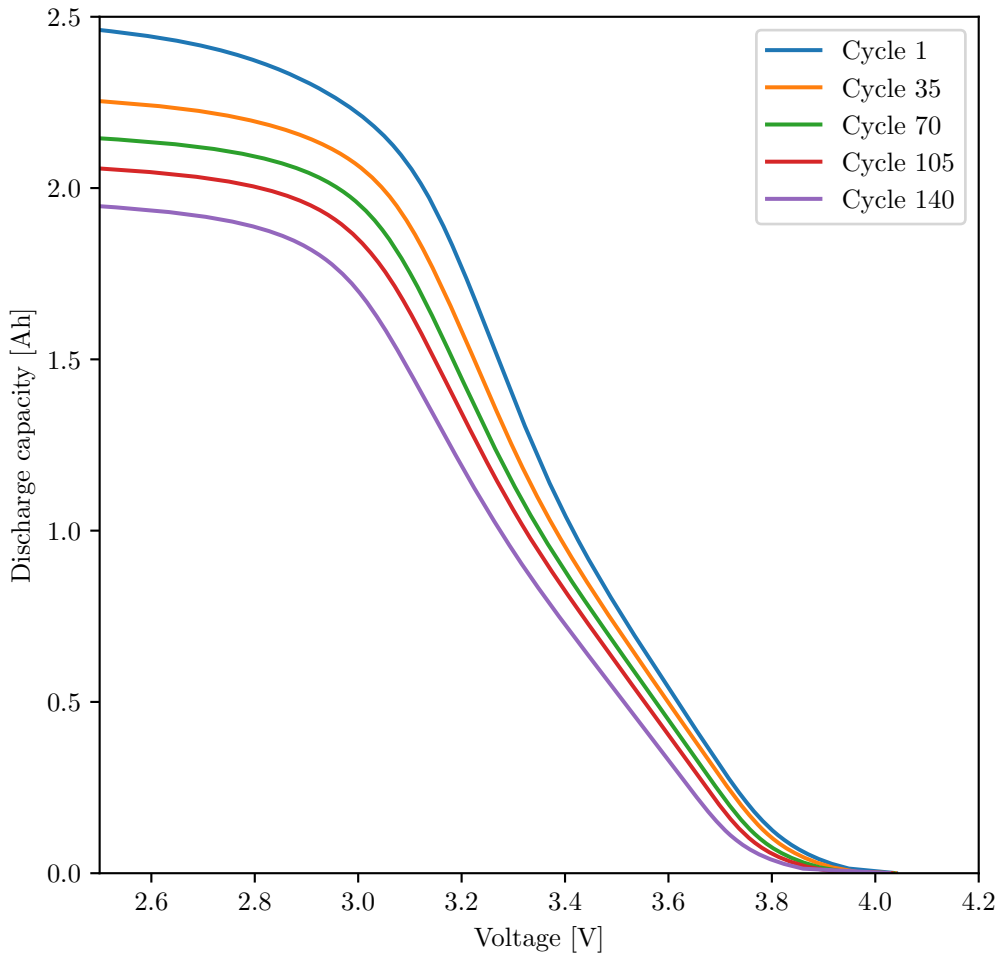

Figure 4.4: $Q(V)$ for five of cell 17's cycles

The discharge capacity voltage curves from cycle 10 and 100 for the four cells are shown in Figure 4.5. As can be seen, they look almost identical to the human eye. Their differential curves are shown in Figure 4.6, where small differences can be noticed.

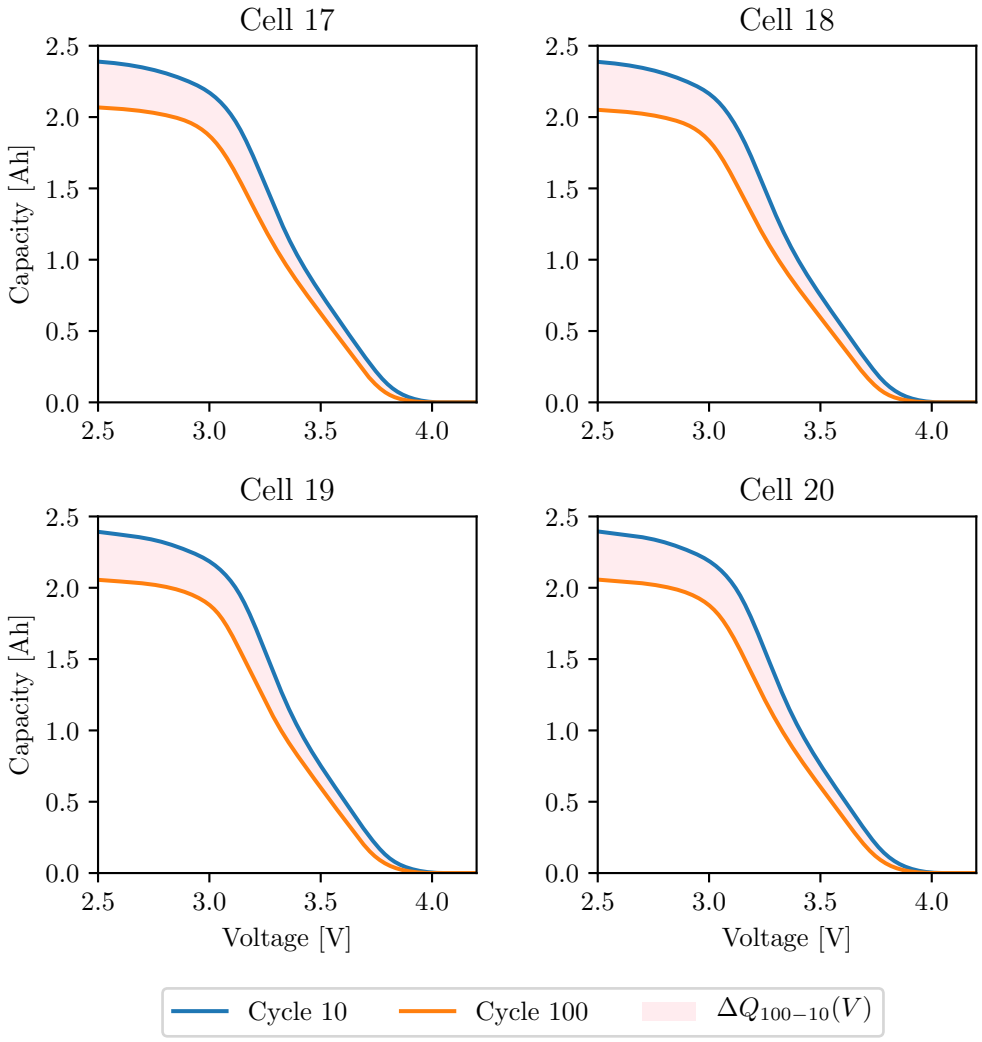

Figure 4.5: $Q(V)$ curves

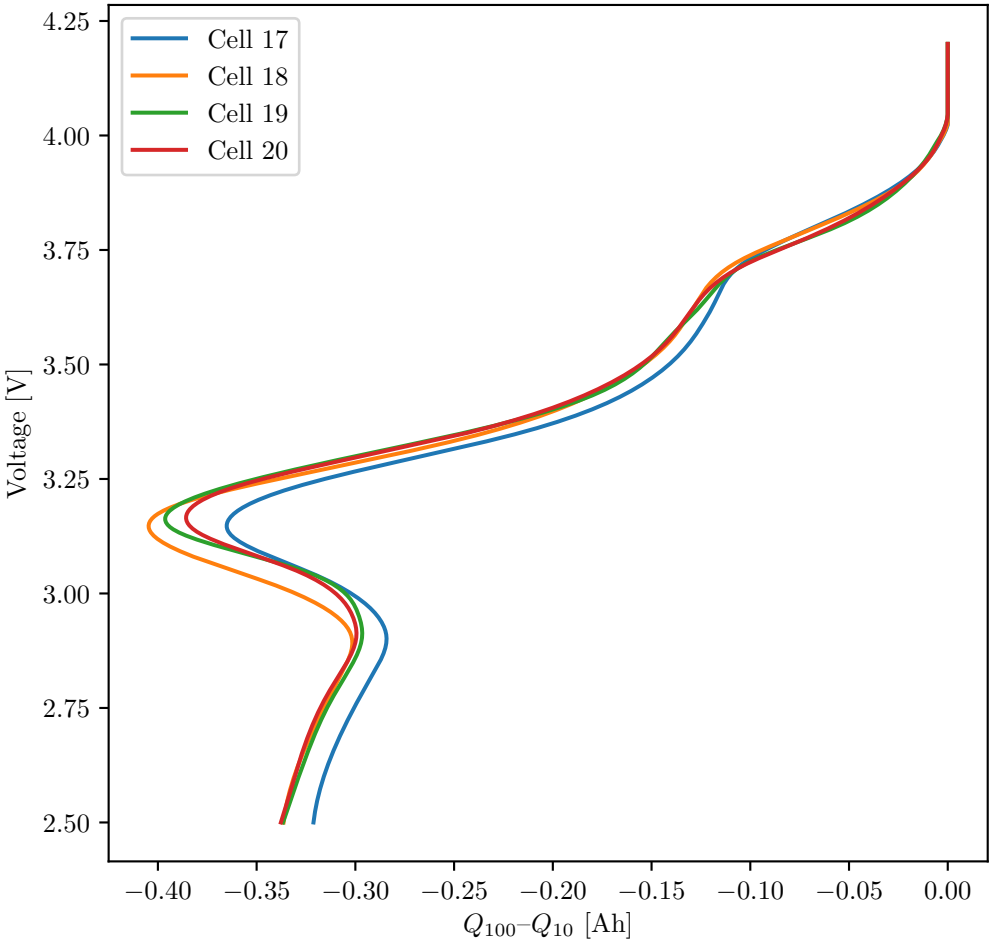

Figure 4.6: $\Delta Q_{100-10}(V)$ curves

The cycle lives and the variance of the differential curves for the HE4 cells are plotted in Figure 4.7. For comparison, the same data for the M1A cells is included as well.

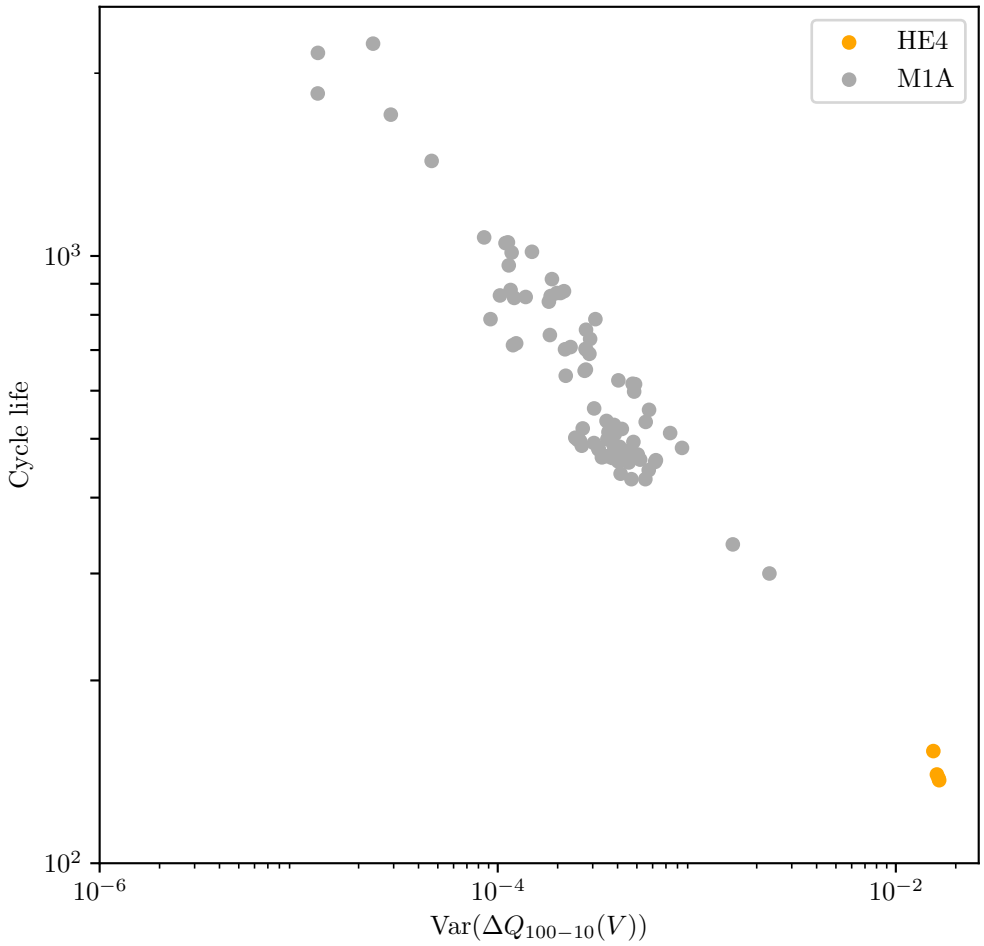

Figure 4.7: Cycle life as a function of $\mathrm{Var}(\Delta Q_{100-10}(V))$ for M1A and HE4 cells on logarithmic axes

Table 4.2 lists the model's predicted cycle lives and the errors compared to the actual cycle numbers.

Cell	17	18	19	20
Actual	153	137	138	140
Predicted	125.90	118.33	119.86	120.23
Error	27.10	18.67	18.14	19.77

Table 4.2: Model cycle life predictions

The RMSE for these predictions is 21.23 cycles, which gives a MPE of 14.65 %.

The M1A cells, used in the reference study, had an average cycle life of 806 cycles, which means that the RUL prediction was made after 12.4 % of their average total lifetime. For the HE4 cells, this would correspond to making the prediction after 17 cycles. To see how the model performs when using data from earlier cycles, the MPE as a function of cycle index combinations is plotted in Figure 4.8, where i and j are the cycle indices ($i > j$) in the differential discharge capacity curve $Q_{i-j}(V)$. The color scale is logarithmic to highlight the contrasts.

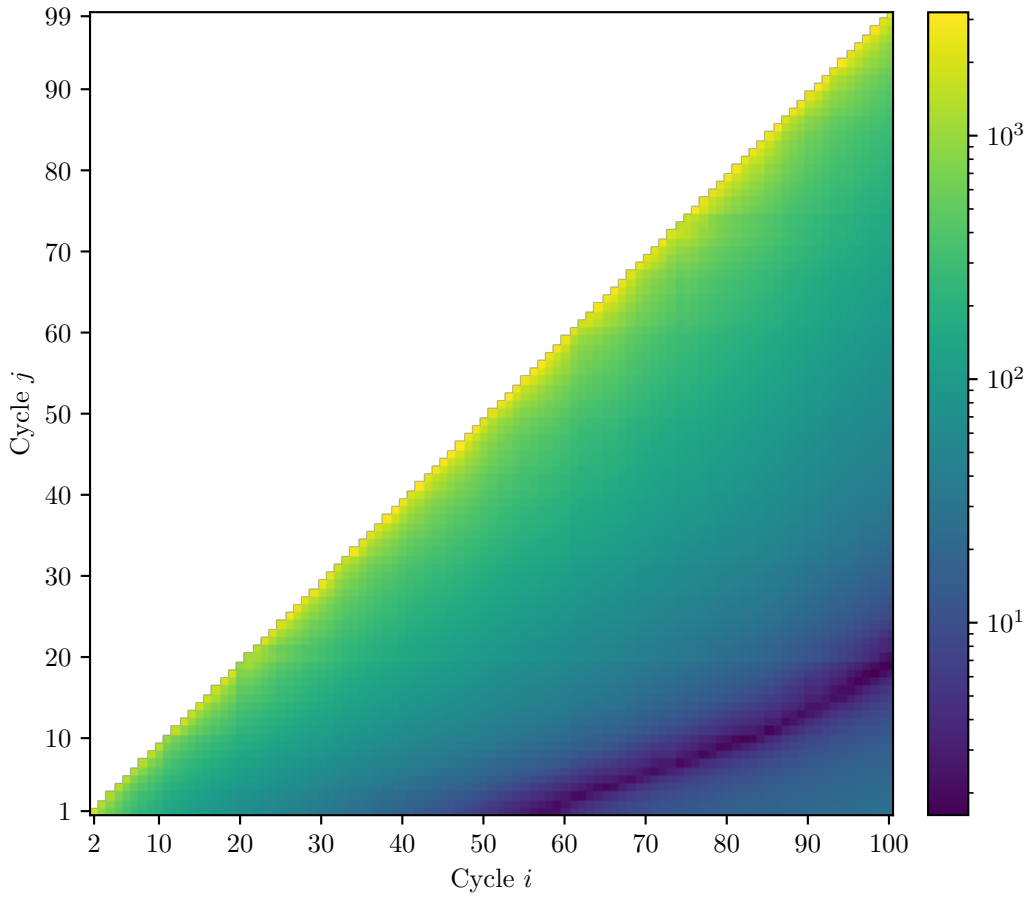

Figure 4.8: MPE as a function of cycle indices i and j for cycle life prediction of HE4 cells

5

Discussion

Even if cell 17 and 18 were cycled with the same cycling protocol, cell 17 performed 16 more cycles than cell 18 before reaching 80 % SoH. This is however not a particularly surprising outcome since cells will never be exactly the same due to minor differences in the manufacturing process, the structure and amount of the active materials, etc. This is also reflected in Table 4.1, where the capacities are unique for all cells.

The HE4 and M1A cells have different rated capacities and voltage ranges because of the different cell chemistries. This also affects the discharge capacity voltage curves as well as the differential curves, which are noticeably different from those of the M1A cells. During discharge, the M1A cells' voltage remains near 3.1 V during the majority of the SoC window. The HE4 cells' voltage, however, decreases almost linearly from 3.8 to 3.1 V.

Despite their dissimilarities, the model was able to give a useful prediction of the cells' cycle lives.

The prediction error of 21 cycles may not seem very much. However, compared to the total number of cycles the HE4 cells performed, 21 out of 142 cycles equals almost a seventh. This is a relatively big portion of the cells' cycle lives. That is why the MPE of 14.65 % is higher than the MPE of 11.4 % obtained when the model is evaluated on the test dataset of the M1A cells.

The prediction after 100 cycles is quite close to the cell's EoL. 70 % of their cycle life has by then already passed, which may or may not be useful depending on the application. Either way, an earlier prediction is preferable.

As can be seen in Figure 4.8, better RUL predictions can be made sooner. The purple area shaped as a curved line in the lower right-hand corner of the figure represents combinations of cycle indices giving prediction errors below 10 %. Using cycle 10 as the first cycle index, data from cycles close to cycle 80 results in predictions with the lowest errors. If cycle 6 were to be used as the first cycle instead, the lowest prediction errors are acquired when combining it with data from cycles around cycle 70. It can also be seen that even cycles between 50 and 60 give accurate predictions using data from the first discharge. This means that precise predictions can be made

when 40 % of the cells' average cycle life has passed, which is a big improvement compared to making a prediction after 100 cycles, when only 30 % of the cells' cycle life remains. However, to make good predictions already after cycle 17, at the same point in lifetime as for the M1A cells, is not possible for the HE4 cells using this model and its training data.

The C-rates in the cycling protocols were converted to currents assuming that the initial capacity of the cells was 2.5 Ah. However, this was not the case given the measurements of the first cycle. Considering that the initial capacity was on average about 3 % above the rated capacity, the currents were slightly lower than intended. As a consequence, the cells may have lived marginally longer. This should not have any impact on the accuracy of the model's predictions though since the currents remained the same during the whole experiment and since the model's predictions were not based on the C-rates or the currents.

It can be seen in Figure 4.6 that the negative peak between 3.0 and 3.25 V have different magnitudes for the different cells. The order of cycle lives is reflected in the order of the peak magnitudes. Cell 18, the shortest lived cell, has the highest peak (the lowest $Q_{100-10}(V)$ value) while cell 17, the longest lived cell, has the lowest peak (the highest $Q_{100-10}(V)$ value of the peaks for all cells). This directly affects the variances and thus the predicted cycle lives.

The interrelationship between the cycle life numbers is also present in the predicted number of cycles for the prediction after 100 cycles. This could however be by chance since the sample size is very small. On the contrary, this pattern is also visible in predictions made from data prior the 100th cycle, indicating that this in fact is related to the cells' degradation.

In contrast to the experiment by Severson et al., no temperature chamber was used. This should not make any big difference since the cooling effect from the axial fans functioned just as well along with the roughly constant ambient temperature throughout the cycling process. What did change was the cell can temperature, which increased as the cells aged due to higher IR. This aligns with the temperature and IR increases of the M1A cells.

Severson et al. did not perform any RPTs on the cells used in the datasets for the model. The on average 13 hours long RPTs after cycle 10 and 100 gave the HE4 cells the opportunity to rest and recover from the fast and aggressive cycling. This most likely prolonged their cycle lives. If no RPTs had been performed, the predictions could have been more accurate, since the input to the model was based on cycles prior these RPTs. How much cannot be said, but presumably not significantly.

6

Conclusions and Future Work

Even if the sample size of this experiment is very small, this work suggests that there is useful information embedded in discharge capacity voltage curves and their differential curves for saying something about aging of this type of NMC cell. This may also be the case for other NMC cells and possibly other lithium-ion batteries. To evaluate that, further experiments with bigger sample sizes, different chemistries and a richer variety of cycling protocols have to be conducted.

This work also strengthens the potential of using large amounts of data with machine learning for predicting cycle life and RUL of lithium-ion batteries. The next step in this direction would be to evaluate the performance of the other machine learning models developed by Severson et al. [1].

In real-life scenarios, outside controlled lab environments, continuous and uniform discharge curves as those obtained in this experiment can generally not be expected. To counter that, and to still be able to use discharge capacity voltage curves as shown in this work with this or a similar model, one can study the possibility of combining fragments of discharge curves from multiple cycles to estimate complete curves over the full intervals of both capacity and voltage.

Bibliography

[1] Kristen A Severson et al. "Data-driven prediction of battery cycle life before capacity degradation". In: *Nature Energy* 4.5 (2019), pp. 383–391.

[2] Sebastian Samuelsson. "Conceptual Design of Propulsion Systems for Boundary Layer Ingestion". PhD thesis. 2019.

[3] R Cecchini and G Pelosi. "Alessandro Volta and his battery". In: *IEEE Antennas and Propagation Magazine* 34.2 (1992), pp. 30–37.

[4] Isidor Buchmann. *Battery Aging in an Electric Vehicle (EV)*. Battery University. 2019. URL: `https://batteryuniversity.com/learn/article/bu_1003a_battery_aging_in_an_electric_vehicle_ev` (visited on 02/18/2020).

[5] Matthew Li et al. "30 years of lithium-ion batteries". In: *Advanced Materials* 30.33 (2018), p. 1800561.

[6] David Coffin and Jeff Horowitz. "The Supply Chain for Electric Vehicle Batteries". In: *J. Int'l Com. & Econ.* (2018), p. 1.

[7] Johannes Kasnatscheew et al. "Do Increased Ni Contents in $LiNi_xMn_yCo_zO_2$ (NMC) Electrodes Decrease Structural and Thermal Stability of Li Ion Batteries? A Thorough Look by Consideration of the Li^+ Extraction Ratio". In: *ACS Applied Energy Materials* 2.11 (2019), pp. 7733–7737.

[8] Peiyi Sun et al. "A Review of Battery Fires in Electric Vehicles". In: *Fire technology* (2020), pp. 1–50.

[9] Jingliang Zhang and Jay Lee. "A review on prognostics and health monitoring of Li-ion battery". In: *Journal of power sources* 196.15 (2011), pp. 6007–6014.

[10] Michel Armand and J-M Tarascon. "Building better batteries". In: *Nature* 451.7179 (2008), pp. 652–657.

[11] Lifeng Wu, Xiaohui Fu, and Yong Guan. "Review of the remaining useful life prognostics of vehicle lithium-ion batteries using data-driven methodologies". In: *Applied Sciences* 6.6 (2016), p. 166.

[12] Thomas B Reddy. *Linden's handbook of batteries*. Vol. 4. McGraw-hill New York, 2011.

[13] Ira Bloom et al. "Differential voltage analyses of high-power lithium-ion cells. 4. Cells containing NMC". In: *Journal of Power Sources* 195.3 (2010), pp. 877–882.

[14] Christoph R Birkl et al. "Degradation diagnostics for lithium ion cells". In: *Journal of Power Sources* 341 (2017), pp. 373–386.

[15] Yuan Zou et al. “Combined state of charge and state of health estimation over lithium-ion battery cell cycle lifespan for electric vehicles”. In: *Journal of Power Sources* 273 (2015), pp. 793–803.

[16] Robert Spotnitz. “Simulation of capacity fade in lithium-ion batteries”. In: *Journal of power sources* 113.1 (2003), pp. 72–80.

[17] Hao Li et al. “An analysis on plug-in electric vehicle’s operating cost considering cost of battery capacity degradation”. In: *2017 IEEE International Conference on Industrial Technology (ICIT)*. IEEE. 2017, pp. 1388–1392.

[18] Sina Sharif Mansouri et al. “Remaining useful battery life prediction for UAVs based on machine learning”. In: *IFAC-PapersOnLine* 50.1 (2017), pp. 4727–4732.

[19] Yapeng Zhou et al. “A novel health indicator for on-line lithium-ion batteries remaining useful life prediction”. In: *Journal of Power Sources* 321 (2016), pp. 1–10.

[20] Heng Zhang et al. “An improved unscented particle filter approach for lithium-ion battery remaining useful life prediction”. In: *Microelectronics Reliability* 81 (2018), pp. 288–298.

[21] Datong Liu et al. “Lithium-ion battery remaining useful life estimation with an optimized Relevance Vector Machine algorithm with incremental learning”. In: *Measurement* 63 (2015), pp. 143–151.

[22] Jerry Barker, Rene Koksbang, and M.Yazid Saidi. “An electrochemical investigation into the lithium insertion properties of Li_xNiO_2 ($0 \leq x \leq 1$)”. In: *Solid State Ionics* 89.1 (1996), pp. 25–35.

[23] Ira Bloom et al. “Differential voltage analyses of high-power, lithium-ion cells: 1. Technique and application”. In: *Journal of Power Sources* 139.1 (2005), pp. 295–303.

[24] Matthieu Dubarry et al. “Capacity and power fading mechanism identification from a commercial cell evaluation”. In: *Journal of Power Sources* 165.2 (2007). IBA – HBC 2006, pp. 566–572.

[25] Caihao Weng et al. “On-board state of health monitoring of lithium-ion batteries using incremental capacity analysis with support vector regression”. In: *Journal of Power Sources* 235 (2013), pp. 36–44.

[26] Linfeng Zheng et al. “Incremental capacity analysis and differential voltage analysis based state of charge and capacity estimation for lithium-ion batteries”. In: *Energy* 150 (2018), pp. 759–769.

[27] Xiaoyu Li et al. “State-of-health estimation for Li-ion batteries by combing the incremental capacity analysis method with grey relational analysis”. In: *Journal of Power Sources* 410 (2019), pp. 106–114.

[28] Elie Riviere et al. “$LiFePO_4$ Battery State of Health Online Estimation Using Electric Vehicle Embedded Incremental Capacity Analysis”. In: *2015 IEEE Vehicle Power and Propulsion Conference (VPPC)*. IEEE. Aug. 2015, pp. 1–6.

[29] Hui Zou and Trevor Hastie. “Regularization and variable selection via the Elastic Net”. In: *Journal of the Royal Statistical Society, Series B* 67 (2005), pp. 301–320.

A

Test Regimes

Since the available capacity of the cells decreases as the cells age, the capacities at SoC levels Q_1 and Q_2 also change accordingly during the cycling process. Therefore, after each cycle, the variables were re-computed based on how many mAh the cell delivered during that cycle. This corresponds to instructions 32-39 in the test regime of protocol A (Figure A.1).

At SoC level Q_2, an IR test was carried out by applying ± 4 A in ten 30 ms long pulses.

Before and after the IR tests and after reaching 100 % respectively 0 % SoC, the cells rested for 5 seconds.

After cycle 10 and cycle 100, a RPT was performed. First, the cells rested for 2 hours. The cells were then charged with CC-CV at 0.5C with a cut-off of 50 mA. Lastly, the cells were discharged with CC at 0.1C until the voltage hit 2.5 V.

Neither the results of the RPTs nor the IR measurements were used in this study, but they provide useful information to further analysis of the experiment.

Test regimes in the program MWare are divided into blocks. The cycling protocols in this project had the following block structure:

0. Satefy checking – Assure sensors are connected and initialization of `Q1` and `Q2`.
1. Initial discharge – Discharge with 1C to 2.5 V using CC-CV for 10 hours.
2. Cycle 1-10 – First 10 cycles with fast charging protocols.
3. RPT – First RPT.
4. Cycle 11-100 – Remaining cycles up to 100.
5. RPT – Second RPT.
6. Cycle 101-200 – Next 100 cycles.

Block 2 and 3 for protocol A are shown in Figure A.1 and Figure A.2.

18:	**I Charge**	2.36C	
	`AhChr` > `Q1`	Goto next	
19:	**I Charge**	1.78C	
	`AhChr` > `Q2`	Goto next	
20:	**Idle**	5 s	
21:	**I Charge**	4 A	30 ms
22:	**Idle**	30 ms	
23:	**I Disch.**	4 A	30 ms
24:	**Idle**	30 ms	
25:	**Loopback Step**	21	4
26:	**Idle**	5 s	
27:	**I Charge**	1C	
	`Voltage` > 4.2 V	Goto next	
28:	**V Charge**	4.2 V	
	`Current` < 100 mA	Goto next	
29:	**Idle**	5 s	
30:	**I Disch.**	4C	
	`Voltage` < 2.5 V	Goto next	
31:	**V Disch.**	2.5 V	
	`Current` < 50 mA	Goto next	
Formula: `Q1` = `AhDisch` * 54 / 100			
32:	**Change variable 2**	`Var32` = `AhDisch`	
33:	**Change variable**	`Var32` * 54	
34:	**Change variable**	`Var32` / 100	
35:	**Change variable 2**	`Q1` = `Var32`	
Formula: `Q2` = `AhDisch` * 80 / 100			
36:	**Change variable 2**	`Var32` = `AhDisch`	
37:	**Change variable**	`Var32` * 80	
38:	**Change variable**	`Var32` / 100	
39:	**Change variable 2**	`Q2` = `Var32`	
Increment Cycle			
40:	**Change variable**	`CycleNr` + 1	
41:	**Change variable**	`AhChr` = 0	
42:	**Change variable**	`AhDisch` = 0	
43:	**Idle**	5 s	
44:	**Loopback Step**	18	9

Figure A.1: Instruction block 2: cycles 1-10 in protocol A. Irrelevant parts have been omitted.

45:	**Idle**	2 h
46:	**I Charge**	0.5C
	`Voltage` > 4.2 V	Goto next
47:	**V Charge**	4.2 V
	`Current` < 50 mA	Goto next
48:	**Change variable 2**	`Q_RPT_ch` = `AhChr`
49:	**Idle**	10 s
50:	**I Disch.**	0.1C
	`Voltage` < 2.5 V	Goto next
51:	**V Disch.**	2.5 V
	`Current` < 50 mA	Goto next
52:	**Change variable 2**	`Q_RPT_dch` = `AhDisch`
Increment Cycle		
53:	**Change variable**	`CycleNr` + 1
54:	**Change variable**	`AhChr` = 0
55:	**Change variable**	`AhDisch` = 0

Figure A.2: Instruction block 3: the first RPT. Irrelevant parts have been omitted.

B

Charging Protocol Flowchart

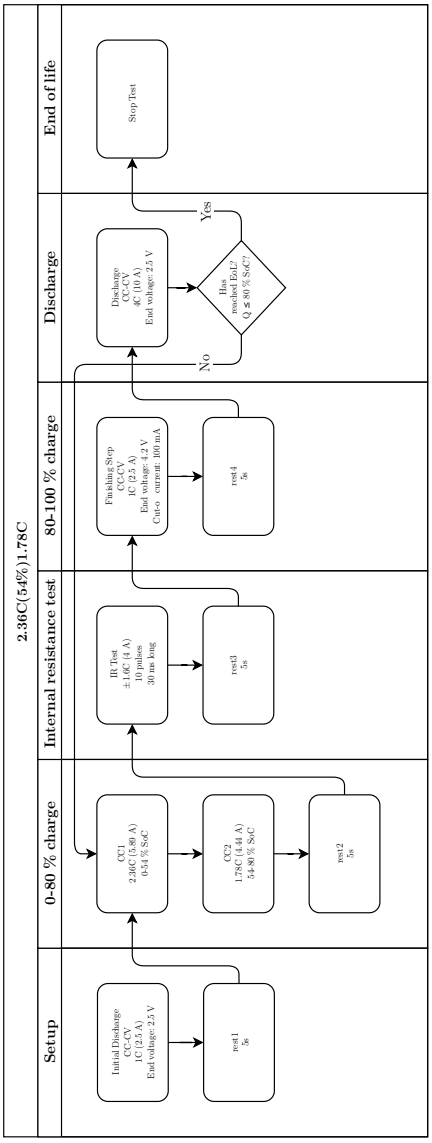

Figure B.1: Flowchart of charging protocol A